Unsteady computational fluid dynamics in front crawl swimming

Mathias Samson, Anthony Bernard, Tony Monnet, Patrick Lacouture, Laurent David

Unsteady Computational Fluid Dynamics in front crawl swimming.

Mathias SAMSON, Anthony BERNARD, Tony MONNET, Patrick LACOUTURE, Laurent DAVID

Institut Pprime, UPR 3346, CNRS, Université de Poitiers, France.

ABSTRACT

The development of codes and power calculations currently allows the simulation of increasingly complex flows, especially in the turbulent regime. Swimming research should benefit from these technological advances to try to better understand the dynamic mechanisms involved in swimming. An unsteady Computational Fluid Dynamics (CFD) study is conducted in crawl, in order to analyse the propulsive forces generated by the hand and forearm. The k-ω SST turbulence model and an overset grid method have been used. The main objectives are to analyse the evolution of the hand-forearm propulsive forces and to explain this relative to the arm kinematics parameters. In order to validate our simulation model, the calculated forces and pressures were compared with several other experimental and numerical studies. A good agreement is found between our results and those of other studies. The hand is the segment that generates the most propulsive forces during the aquatic stroke. As the pressure component is the main source of force, the orientation of the hand-forearm in the absolute coordinate system is an important kinematic parameter in the swimming performance. The propulsive forces are biggest when the angles of attack are high. CFD appears as a very valuable tool to better analyze the mechanisms of swimming performance and offers some promising developments, especially for optimizing the performance from a parametric study.

Keywords: URANS method, CFD, propulsive forces, k-ω SST turbulence model, VOF method.

1. Introduction

In competitive swimming, the hand and forearm play a major role in the propulsion of the swimmers (Maglischo 2003; Takagi and Sanders 2002). Moreover Berger et al. (1995), Toussaint et al. (2002) and Kudo et al. (2013) highlight the leading role of the hand relative to the forearm (67 % of the hand-forearm propulsive force according Schleihauf et al., 1983). The propulsive forces are created by the flow surrounding the swimmer's arms. The hand motions in front crawl swimming are complex: it is three-dimensional with sudden changes in velocities and angles of attack (Samson et al. 2015). Thus, the induced flow is highly non-linear and turbulent containing complex unsteady vortex dynamics (Toussaint et al. 2002; Polidori et al. 2006; Zaïdi et al. 2010; Takagi et al. 2015). It is therefore extremely difficult to study, both experimentally and numerically. Nevertheless, progress in recent years, not only in the development of numerical methods and turbulence modelling, but also in computing power, currently allows to simulate more complex flows. CFD is seen as an interesting tool because it allows to simulate, the flow around a given geometry, and the external forces applied to the solid parts. Bixler and Schloder (1996) have shown that studies conducted in CFD in quasi-static conditions are insufficient to model a complex flow around a swimmer. Indeed, these methods take into account the average of the flow field, without taking into account the unsteady effects, engendered by the fast instantaneous velocity variations (Sato and Hino 2013; Rouboa et al. 2006). These effects, however, play a major role in the overall dynamics of the flow. The first unsteady effect highlighted in swimming was the mass effect added (Pai and Hay 1988). Ellington in 1984 defines it as is the reaction force due to the acceleration and deceleration of the fluid particles around the moving solid. A second effect (bound vortex), which is the circulation around a body following a vortex shedding, plays an important role in swimming, especially during the phases of change of direction of the hand (Takagi et al. 2014). These two effects favorably contribute to the thrust.

Recently, unsteady studies have been proposed to analyse the flow around the swimmers. Lecrivain et al. (2010) have numerically investigated the effect of body roll amplitude and of upper arm rotation speed on the propulsion of an arm amputee swimmer. Keys et al. (2010), from a smoothed particle hydrodynamics (SPH) method, examined propulsive and drag forces experienced

across the body during full-body freestyle swimming. Both used the morphing mesh method to model the joint segment, with the k-ε turbulence model. Moreover, Sato and Hino (2013) simulated, by a moving mesh method, a flow surrounding a hand but without turbulence model or free surface. Turbulence models and the local Reynolds number are very important in the simulation because the role played by the boundary layer in the creation of turbulence. Turbulence models have been improved a lot in recent years, in particular by taking more account of near wall phenomena (Manceau 2010). So, the turbulence models used in the research of swimming have progressed from a k-ε turbulence model with Bixler (2002), to a k-ω model more recently with Popa et al. (2014) and Arfaoui and Polidori (2014). These two eddy-viscosity models are the most popular in CFD studies in this domain. Banks et al. (2014) used the Shear Stress Transport (SST) k-ω turbulence model (Menter 1994) to measure the passive drag around a swimmer. This model better reflects the physics than k-ε model, because it combines the qualities of the high Reynolds k-ε model (away from walls), and the low Reynolds k-ω model (near the walls).

In this context, an unsteady CFD study is presented that applies the URANS method (Unsteady Reynolds Averaged Navier-Stokes). This method is widely used in aeronautics, and although it remains a subject of active research, it has been validated in many canonical unsteady flows: wake, downward–step, and compressible co-axial jets (Fadai-Ghotbi 2007). To better approximate the physics of the flow, we propose a free surface modeled by a Volume of Fluid method (VOF), and we use the k-ω SST turbulence model. We employ a polyhedral finite-volume Navier-Stokes flow solver, coupled with of an overset mesh method. The main purpose was dual: first to analyse the evolution of the hand-forearm propulsive forces, and explain this relative to the arm kinematics parameters. Second, to validate this model by comparaison with others results.

2. Methods

2.1. Numerical method

URANS method

The flow around a swimmer is turbulent and unsteady with high Reynolds number, thus a full Direct Numerical Simulation (DNS) is not possible with today's computing power. A method to resolve this shortcoming is to use the Reynolds averaged Navier Stokes equations, closed by a turbulence model, under the unsteady form (URANS equations). These equations are obtained by introducing the Reynolds decomposition, which takes into consideration that, in turbulent flows, each instantaneous variable is the sum of a mean component and a fluctuating component (equations (1), (2)):

$$U_i(x,t) = < U_i(x,t) > + u_i'(x,t) \quad \textbf{(1)}$$

$$< U_i(x,t) > = \lim_{N\to\infty} \frac{1}{N+1} \sum_{n=0}^{N} U_i(x, t + nT) \quad \textbf{(2)}$$

$U_i(x,t)$ is the instantaneous velocity of the hand component in the i-direction (m/s), $< U_i(x,t) >$ is the phase average of velocity component in the i-direction (m/s), $u_i'(x,t)$ is the fluctuating velocity component in the i direction (m/s). Equation (1) is obtained from the double decomposition (Cantwell and Coles 1983). In the equation 2, T is the period of the cyclic phenomenon, i.e. from the entry of the hand into the water to the exit.

Then, the time averaging of the instantaneous equations leads to the following system of averaged equations ((3) and (4)). These equations are formally identical to the RANS equations for a statistically unsteady flow, taking into account the unsteady term $\frac{\partial < U_i >}{\partial t}$.

$$\frac{\partial < U_i >}{\partial x_i} = 0 \quad \textbf{(3)}$$

$$\frac{\partial \langle U_i \rangle}{\partial t} + \langle U_j \rangle \frac{\partial \langle U_i \rangle}{\partial x_j} = -\frac{1}{\rho}\frac{\partial \langle P \rangle}{\partial x_i} + g_i + \nu \frac{\partial^2 \langle U_i \rangle}{\partial x_j \partial x_j} - \frac{\partial \langle u_i' u_j' \rangle}{\partial x_j} \quad \textbf{(4)}$$

This URANS decomposition can be interpreted as the application of an implicit spatio-temporal filter at instantaneous variables, this filter being employed by the introduction of a turbulence model in the equations. The filter $< U(x,t) >$ must extract the large-scale organised vortex structures to calculate it, while the fluctuation $u'(x,t)$, representative of turbulent agitation, is modeled. The term $< u'_i \, u'_j >$, called the inconsistent Reynolds tensor, represents the influence of the background turbulence (modeled) on the filtered field (resolved).

Turbulence model

The k-ω SST turbulence model was used for closing the URANS equations. This is a two-equation eddy-viscosity model, in which k is usually interpreted as the turbulence kinetic energy and ω is the rate of dissipation of the eddies. k-ω SST is a "hybrid" of two models: the k–ω model (Wilcox, 1988) which is efficient in the near-wall region (but not applicable to external aerodynamics) and the standard k–ε model (Launder and Spalding, 1974) which gives good results far from the wall. The transition between the two models is made by quite complex functions which depend on the distance to the wall. This model has been preferred to other low-Reynolds models (as the low-Reynolds k-ε model for instance) because k-ω SST is integrable down to the wall, without introducing a damping function, which allows to take more account of the geometry of the solid. Moreover the equation of ω is independent of that of k, which is a factor of numerical robustness.

These parameters are defined from two transport equations:

$$\frac{\partial k}{\partial t} + U_j \frac{\partial k}{\partial x_j} = P_k - \beta^* k\omega + \frac{\partial}{\partial x_j}\left[(\nu + \sigma_k \nu_T)\frac{\partial k}{\partial x_j}\right] \quad \textbf{(5)}$$

$$\frac{\partial \omega}{\partial t} + U_j \frac{\partial \omega}{\partial x_j} = \alpha S^2 - \beta \omega^2 + \frac{\partial}{\partial x_j}\left[(\nu + \sigma_\omega \nu_T)\frac{\partial \omega}{\partial x_j}\right] + 2(1 - F_1)\sigma_{\omega 2}\frac{1}{\omega}\frac{\partial k}{\partial x_i}\frac{\partial \omega}{\partial x_i} \quad \textbf{(6)}$$

ν_T (kinematic eddy viscosity) is calculated as a function of *k* and *ω* by the following equation:

$$\nu_T = \frac{a_1 k}{\max(a_1 \omega, SF_2)} \quad \textbf{(7)}$$

F1 and F2 are blending functions, and the clothing coefficients are:

α1	α2	β1	β2	β*	σ_{k1}	σ_{k2}	$\sigma_{\omega 1}$	$\sigma_{\omega 2}$
5/9	0.44	0.075	0.0828	0.09	0.85	1	0.5	0.856

(8)

The use of a k-ω SST formulation in the inner parts of the boundary layer makes the model directly usable all the way down to the wall through the viscous sub-layer. It requires a higher resolution mesh to solid boundaries (see below) with the first calculation point in the viscous sublayer.

Flow solver

The numerical simulations have been carried out with the STAR-CCM+® software. The finite volume method is applied on a hybrid mesh made of structured mesh (near-wall) and unstructured mesh. The computation is made from a computer with 736 processors at 2.7 GHz and 1.47 TB of RAM. The linkage between the momentum and continuity equations is achieved with a predictor-corrector approach, with a standard SIMPLE algorithm. The advancement in time is done by an implicit first-order Euler scheme. This physical time-step was $2.5.10^{-3}$ s (with 30 inner iterations) and was chosen to obtain a Courant–Friedrichs–Lewy number ($U\Delta x/\Delta t$) close to 1 when U is maximal.

Free surface

The free surface is simulated with multi-phase liquid and air of constant density from a Volume of Fluid method (VOF). According to Dabnichki (2011), the presence of the free surface should affect the force generation especially in the initial and final phases when the arm is close to the surface.

Overset grid method

This method consists to move a mesh (overset) into a fixed mesh (background). The overset grid method enables to efficiently simulate a movement of solid body (here the hand-forearm) in a fluid. The volumes

control domain consisted of two regions (Figure 1): the background (parallelepiped 5m x 3m x 1m, containing 280,000 cells), fixed, and an overset (sphere of 1m in diameter containing 820,000 cells), attached at the hand-forearm and moving with it with six degrees of freedom (three in rotation and three in translation). The mesh consisted of polyhedral and pyramidal cells. It was refined and structured at the near wall of the hand-forearm, using 10 prism layers, stretching at 1.1, which the size of the first cell is equal to 10^{-4} m to obtain $y^+ \approx 1$. y^+ being a dimensionless number equal to yu_τ/ν , with u_τ the friction velocity ($u_\tau = \sqrt{\tau_p/\rho}$, τ_p : wall shear stress, ρ: fluid density).

Figure 1

The mesh is also refined at the free surface. Beyond the near wall areas, the mesh is unstructured in the overset volume. The background mesh is structured, with average mesh size equal to 0.07 m. The independence of the calculated physics based on the numerical conditions was tested with respect to the computational time-step, the number of iterations, and the domain and mesh size. The interface between the two regions was then calculated by interpolation between active cells near each region.

Boundary conditions

Two *inlet* boundaries were defined (Figure 1). A first, vertical, composed of an air / water in variable composition (managed by a field function), the input velocity is equal to 0 $m.s^{-1}$ for reproducing the condition of a fluid at rest. The second (top surface) consists only of air. An *outlet* boundary (in pressure condition) is composed of an air / water varying in composition to ensure the conservation equations. Both sides of the volume are defined as a *symmetry plane*. The surface of the arm and the bottom of the volume are defined as a *wall* to obtain no-slip conditions. The free surface is set at a height of 2 m above the pool bottom.

2.2. Kinematic parameters of the simulation

Geometry of the hand-forearm surface

The simulation consisted of reproducing the trajectory of a hand-forearm of a swimmer in sprint pace, from experimental kinematics measurements. The hand and forearm segment (with the wrist locked) of an expert swimmer (level: 90.2 % of world record, height: 1.80 m, weight: 76 kg) were scanned and digitized by a Minolta VI-900 scanner. A profile was added to the back of the forearm in order to reduce drag arising from the base of the solid (Figure 2). The projected area of hand and forearm are respectively 0.018 m^2 and 0.037 m^2.

Figure 2

Kinematic of the hand-forearm stroke

Kinematic parameters were imported into the solver via a data file, which the time step is equal to the physical time-step ($2.5.10^{-3}$ s). The path analysis began when the tip of the hand entered into the water and finished when it exited. Kinematic data were measured in the context of swimming. A Vicon® optoelectronic motion analysis system was used (Monnet et al., 2014). Eight cameras were placed around a specific pool: two under a bottom window and six in front of a lateral window. The light emitted by the LEDs was reflected back to the sensor by passive markers (fixed on the hand and forearm of the swimmer) covered with specific retroreflective tape. The 3D coordinates of the markers were reconstructed based on the 2D image of two or more cameras whose locations and internal parameters are known. Five reflective markers were fixed on the segment (Figure 2): the finger tip (FT), second (M_2) and fifth (M_5) metacarpophalangeal joints, radial styloid (RS) and ulnar styloid (US). Velocity (of the FT point) and hand orientation were expressed in a fixed pool-centric reference system: (X_0, Y_0, Z_0) the X_0-axis points in the swimming direction, the Y_0-axis is perpendicular to the swimming direction pointing from the right to the left of the subject, and the Z_0-axis points vertically upward. A local system of reference (X_h, Y_h, Z_h), linked to the hand-forearm, allowed to calculate the hand orientation (Figure 3). X_h is the axis which passed through FT and the middle (RS, US). Z_h was perpendicular to the (X_h, M_2M_5) plane and Y_h was perpendicular to X_h and Z_h. The orientations of the hand were respectively, the flexion, pronation-supination, and abduction-adduction of the hand-forearm (Figure 3).

Figure 3

Analysis of the hand-forearm stroke

To better study the propulsive forces during the aquatic stroke, the trajectory was decomposed in five phases, in agreement with Maglischo (2003): Enter and stretch (ES, from entry of the hand into the water to the end of the upsweep of the opposite arm), Downsweep to catch (DC, from the end of ES to the most outside point), Insweep (IN, from the end of DC to the most inside point), Upsweep (UP, from the end of IN to the most backward point) and Exit (EX, from the end of UP to the exit of water). This trajectory is shown in figure 4.

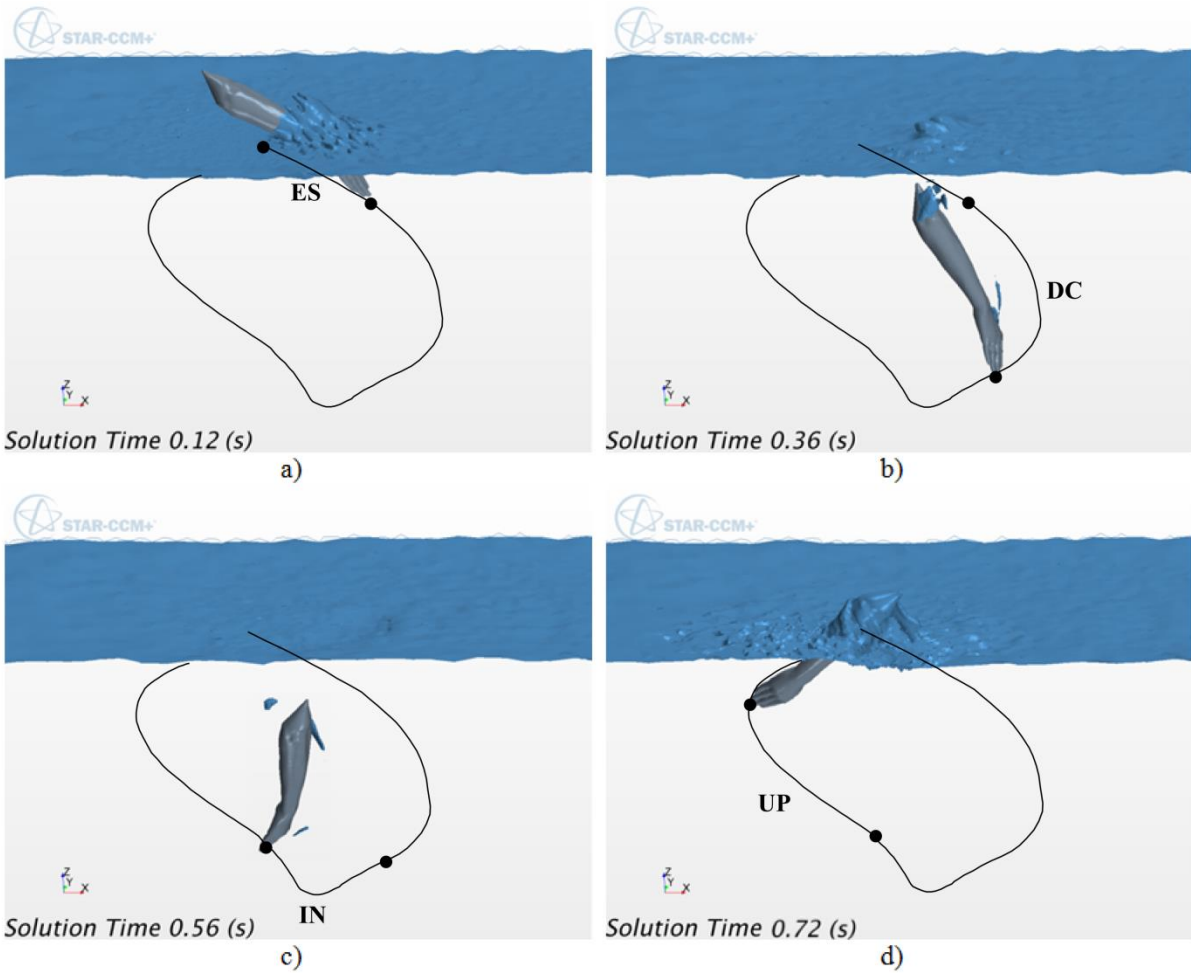

Figure 4. Illustration of the hand-forearm segment path with the free surface, as well as the different phases of the aquatic stroke: a) ES phase; b) DC phase; c) IN phase; d) UP phase.

The five phases of the water path (ES, DC IN, UP and EX) are highlighted by shaded and unshaded areas on the figures.

Hand-forearm kinematic parameters

According to Samson et al. (2015), some kinematic parameters are directly responsible forces generated by water on the hand and forearm. Five main parameters were defined: velocity, acceleration, and orientation of the hand in the absolute reference system, and the angles of attack and sweepback. In the context of this simulation, these parameters are defined in figure 5.

Figure 5

2.3. Analysis methodology of the simulation

The aim of the study is twofold:

1- Study the propulsive forces generated by the hand and forearm during the aquatic stroke and explain it in relation to the kinematic parameters previously defined.

2- Compare the results of the simulation to other similar studies.

For this we will rely on the pressure, force and vorticity field calculated. The propulsive forces result from the action of the flow of water on the surface of the hand and the forearm. Often the resulting forces are expressed in a local reference frame of the flow, making possible a discussion of contributions in lift and drag (Schleihauf 1979, Gourgoulis et al. 2015). We will make the choice in this study to decompose the hydrodynamic forces into a pressure component (normal to the wall) and a friction component (tangential to the wall) which represent the two contributions of the surface forces (Anderson, 2010). The aim is in particular to discuss the resulting forces directly from the orientations

of the hand and the forearm. Thus drag and lift forces and pressure and friction forces do not express in the same reference frames making their comparison difficult.

3. Results

The main analysis is to jointly study the spatio-temporal evolution of kinematic hand parameters (Figure 5) and the propulsive forces generated by the hand and forearm (Figure 6). The study combines analysis by phase and the comparison with other studies.

Figure 6

Entry and stretch

During the entry and stretch phase (from t = 0 s to t = 0.12 s, Figure 6), the total propulsive force is negative (close to - 5 N), and represents the drag force generated by the hand-forearm. This product with low angles of attack, the hand palm directed towards the pool bottom (Figure 4 b, d), which generates few forces.

Downsweep to catch

Propulsion begins during the downsweep to catch phase, before the foremost point of the path (at t = 0.26 s). A first peak force is reached at t = 0.32 s (101 N), with the forearm as the main contribution (Figure 6). At this time, there is a significant deceleration of the hand (for the X_0 component, which passes from -23 to 6 $m.s^{-2}$ between t = 0.24 s and t = 0.28 s, Figure 4 b), and a rapid increase of the angle of attack (from 25° at t = 0.26 s to 50° at t = 0.32 s, Figure 4 c). This increase can be explained by a translational movement of the hand-forearm (due to the stagnation of the angle of flexion close to 60 ° between t = 0.26 s and t = 0.32 s).

In order to better understand the origin of the propulsive forces, a summary of the ressure and friction contributions has been done on the hand and forearm. Results are shown in the Table 1.

Table 1

Results show that the pressure is the main contribution of propulsive forces. This is explained because the flow is turbulent ($Re \approx 10^5$) and in a separated regime owing to the large angles of attack, the skin friction becomes negligible (Dickinson 1996; Anderson 2010, p.79). Thus, the resultant force is approximately perpendicular to the hand-forearm segment. The evolution of the propulsive force during the path can therefore be based mainly on the evolution of the pressure over time on the surface of the hand-forearm segment. A representation of the evolution of these 8 pressures points over time is shown in Figure 7. We chose to subtract the hydrostatic pressure from the static pressure in order to overcome the effect of the water depth to facilitate the analysis of the flow on the surfaces.

Figure 7

It is found that, overall, there are high pressures on the palm of the hand and forearm, and low pressures on the back. It is noted that, at t = 0.26 s, there is an increase of high pressures on the palm of hand-forearm, and a decrease of low pressures on the back.

To validate the numerical method, these pressure results were compared with experimental study by direct pressure measurement, performed under the same conditions: in crawl and in sprint (Toussaint et al. 2002), but for a different swimmer. In this study, pressure was measured at the shoulder, elbow, wrist, dorsal side of the hand, and palm of the hand using modified disposable blood pressure transducers. Calculation of pressure by numerical simulation was carried out in the same locations: on the elbow, back and palm of the hand (Figure 8). In the figure below, results give pressure difference relative the dorsal side of the hand.

Figure 8

We find that the two curves have two peaks corresponding to the two phases of IN and UP. The maximum values are close, 7000 Pa for our study, and 6500 Pa for the study of Toussaint et al. (2002). These two peaks are arranged differently: the largest peak is during the UP phase for Toussaint et al. (2002), and during the IN phase for our study. These differences may be encountered (Maglischo 2003): some swimmers propel themselves further during the IN phase, while others rather during the UP phase.

To go further into the analysis, the results of the propulsive force generated by the hand are compared with two other studies in similar conditions: Kudo and Lee (2010) and Sato and Hino (2013), made respectively from pressure sensors, and numerical simulation from a kinematic measure. The results of both studies and ours are shown in Figure 9. Kudo and Lee (2010) computed the propulsive forces exerted by the hand during submaximal swimming pace from a pressure method: a portable data logger with 12 pressure sensors were placed on the hand. Besides, Sato and Hino (2013) analysed the hydrodynamic forces acting on the hands of the top swimmers at middle-distance pace, by CFD unsteady Navier-Stokes solver based on an unstructured grid method. The hand kinematic parameters were calculated by two video cameras.

Figure 9

Results show that the values of forces, in the three configurations, are similar. The three curves show two peaks force which are respectively 78 N and 42 N for our study, 79 N and 66 N for Kudo and 61 N and 59 N for Sato. The curves in this study (in black) and that of Kudo (in blue) are slightly shifted in time, but have very similar values with dominant propulsive forces during the insweep phase. The lowest

values obtained by Sato and Hino can be explained by the slower pace of swimming than the other two, and also because the authors do not use turbulence model in their simulation.

Insweep phase

According to the table 1, the IN phase is the most propulsive phase of the aquatic stroke (72.5 N in mean). During this phase, the angle of flexion is between 60° and 110° (Figure 4 b), i.e. the hand is close to the perpendicular of the forward direction. Moreover during this phase, the angles of attack are the highest in the arm's trajectory (between 50° and 70°). The maximum of propulsive force is achieved at t = 0.40 s. This maximum corresponds to a high angle of attack (70°, Figure 4 c), and an angle of flexion equal to 60°. During this phase, the main contribution of forces arises from the hand (57.3 N for the hand and 15.2 N for the forearm, Table 1) which confirms the results of Berger et al. (1995). The end of insweep marks the end of the first peak force. The flow, during this phase, quickly passes from the little finger to the thumb and wrist (sweepback angles of 70 °, 180 ° and 300 °). Therefore, since during this phase the hand-forearm segment is close to the vertical with respect to the forward direction and the pressure contribution is important, the resultant of the hydrodynamic forces is mainly in the forward direction. These results are in agreement with those of Gourgoulis et al (2015) who showed, from drag and lift components that the resultant of the hydrodynamic forces was oriented in the forward direction. Furthermore, according to this study, it also appears that the resultant forces are perpendicular to the hand of the swimmer, as it has been shown here.

Upsweep phase

A second peak force is located in the UP phase (Figure 6). UP is the second most propulsive phase (30.8 N in mean, Table 1). The beginning of this phase is a transition effected by a change of direction of the hand (at t = 0.54 s, Figure 4 a, c) and a pronation (from 17° at t = 0.54 to 12 ° at t = 0.64 s, Figure 5 c).

In an effort to verify our numerical model further, a comparison with an experimental study (Takagi et al. in 2014) was made during this IN-UP transition. In this study, measurements were performed for a hand attached to a robotic arm which mimicked a human performing the stroke. The flow fields underwater near the hand were obtained via 2D particle image velocimetry (PIV). Comparison between

this two studies is based on the vorticity tensor, which is defined as the rotational of the fluid velocity field:

$$\Omega_{ij} = \frac{1}{2}\left(\frac{\partial u_i}{\partial x_j} - \frac{\partial u_j}{\partial x_i}\right) \quad \textbf{(10)}$$

Vorticity (Ω) allows one to know the intensity and the direction of rotation of the vortex structures. The comparison of our results with those of Takagi et al. (2014) is shown in Figure 10.

Figure 10

In Figure 10, we see in both cases a vortex shedded and an induced jet, due to the rapid change of direction. Takagi et al. (2014) shown, from pressure measurements on the surface of the profile, that the jet and vortex shedding was responsible of the increase of propulsive forces at that time.

Between t = 0.62 s and t = 0.68 s, the propulsive forces of hand are high due to the high angles of attack (near 50° at t = 0.6 s, Figure 5 d) and angles of flexion which are close to 110° (Figure 5 c). The decreasing of the propulsive forces from t = 0.68 s (Figure 6) corresponds to the decreasing of the angles of attack which passes from 40° to 15° at this moment (Figure 5 d), as well as the increasing of the angle of flexion which quickly passes from 110° to 140° on the same time (Figure 5 c). So, the palm of the hand is more and more directed towards the surface of the water. At t = 0.72 s, the end of UP phase is the most rearward point of the hand trajectory. The propulsive forces are low since the angle of attack is close to 10 ° (Figure 4 d), and the angle of flexion is close to 140 ° (Figure 4 c). It is the preparation of the release of the hand of the water and the beginning of the recovery.

In summary, there are two force peaks during the IN and UP phases. The hand is the segment that contributes most to the propulsion. The most important propulsive forces are obtained with the higher angles of attack and with angles of flexion close to 90°. Besides, from the three experimental and

numerical comparisons made relative to several studies, we can conclude that there is a good agreement with the results of this study.

Limitations of the current study

This new unsteady CFD method opens up many possibilities of studies of the swimming. However, some limitations of this approach must be considered. First, the blocked wrist of the segment does not completely reproduce the kinematics of the forearm. An improvement should be made to provide two degrees of freedom to the wrist. Second, although the eddy-viscosity models gives relevant physical results, it certainly could be improved with second-moment closure models (Reynolds Stress Model, RSM) or Large-Eddy Simulation (LES), or hybrid methods (such as Detached-Eddy Simulation for example). However these models, although constantly improving, are not yet operational for such unsteady flows.

4. Conclusion

Computational fluid dynamics is a valuable tool in the perspective of a better understanding of propulsive or resistive mechanisms in swimming. The development of computational tools and turbulence models allows researchers to obtain results that can approximate the experimental measurements. Thus the URANS methodology was used to model the flow around the hand and forearm in front crawl swimming. It has been shown that there was a close link between hand kinematic parameters and the propulsive forces generated. This tool thus provides new light on the propulsive mechanisms in swimming and offers some promising developments, especially for optimizing swimming performance from a parametric study.

References

Anderson Jr JD. 2010. Fundamentals of aerodynamics (5th Edition). Tata McGraw-Hill Education.

Arfaoui A, Polidori G. 2014. Swimming drafting simulation using a k-omega turbulence model. Comput Meth Biomech Biomed Eng. 17(S1): 156-157.

Banks J, James M, Hudson D, Taunton D, Turnock S. 2014. An analysis of a swimmer's passive wave resistance using experimental data and CFD simulations. XIIth International Symposium on Biomechanics and Medicine in Swimming. Canberra, Australian Institute of Sport, 28 April to 2 May.

Berger MA, de Groot G, Hollander A. 1995. Hydrodynamic drag and lift forces on human hand/arm models. J Biomech. 28(2): 125 – 133.

Bixler B, Schloder M. 1996. Computational Fluid Dynamics: An Analytical Tool for the 21st Century Swimming Scientist. J Swim Res. 11: 4-22.

Cantwell B, Coles D. 1983. An experimental study of entrainment and transport in the turbulent near wake of a circular cylinder. J Fluid Mech. 136: 321-374.

Dabnichki P. 2011. Unsteady fluid mechanics effects in water based human locomotion. Math Comput Simulation. 82 : 471–482.

Dickinson MH. 1996. Unsteady Mechanisms of Force Generation in Aquatic and Aerial Locomotion. Amer Zool. 36: 537-554.

Fadai-Ghotbi A. 2007. Modélisation de la turbulence en situation instationnaire par approches URANS et hybride RANS-LES. Prise en compte des effets de paroi par pondération elliptique. PhD thesis report, University of Poitiers.

Gourgoulis V, Boli A, Aggeloussis N, Antoniou P, Toubekis A, Mavrommatis G. 2015. The influence of the hand's acceleration and the relative contribution of drag and lift forces in front crawl swimming. J Sports Sci. 33(7): 696-712.

Keys M, Lyttle A, Blanksby BA, Cheng L. 2010. A Full Body Computational Fluid Dynamic Analysis of the Freestyle Stroke of a Previous Sprint Freestyle World Record Holder. XIth International Symposium for Biomechanics and Medicine in Swimming. Oslo, 16th -19th June.

Kudo S, Lee M. 2010. Prediction of propulsive force exerted by the hand in swimming. In Kjendlie PL, Stallman RK, Cabri J. editors. Biomechanics and Medicine in Swimming XI, 112–114. Norwegian School of Sport Science, Oslo, Norway.

Kudo S, Vennell R, Wilson B. 2013. The effect of unsteady flow due to acceleration on hydrodynamic forces acting on the hand in swimming. J Biomech. 46(10): 1697 – 1704.

Launder BE, Spalding DB. 1974. The numerical computation of turbulent flows. Comp Meth Appl Mech Engng. 3(2):269–289.

Lecrivain G, Payton CJ, Slaouti A, Kennedy I. 2010. Effect of body roll amplitude and arm rotation speed on propulsion of arm amputee swimmers. J Biomech. 43: 1111–1117.

Maglischo EW. 2003. Swimming Fastest, Human Kinetics.

Manceau R. 2011. Modélisation de la turbulence. Habilitation à diriger les recherches. University of Poitiers.

Menter FR. 1994. Two-Equation Eddy-Viscosity Turbulence Models for Engineering applications, AIAA Journal. 32(8): 1598-1605.

Monnet T, Samson M, Bernard A, David L, Lacouture P. 2014. Measurement of three dimensional hand kinematics during swimming with a motion capture system: a feasibility study. Sports Engng. 17:171-181.

Pai YC, Hay JG. 1988. A hydrodynamic study of the oscillation motion in swimming. Int J Sport Biomech. 4: 21–37.

Polidori G, Taiar R, Fohanno S, Mai TH, Lodini A. 2006. Skin-friction drag analysis from the forced convection modeling in simplified underwater swimming. J Biomech. 39: 2535-2541.

Rouboa A, Silva A, Leal L, Rocha J, Alves F. 2006. The effect of swimmer's hand/forearm acceleration on propulsive forces generation using computational fluid dynamics. J Biomech, 39: 1239–1248.

Samson M, Monnet T, Bernard A, Lacouture P, David L. 2015. Kinematic hand parameters in front crawl at different paces of swimming. J Biomech. 48: 3743–3750.

Sato Y, Hino T. 2013. Computational Fluid Dynamics Analysis of Hydrodynamic Force Acting on a Swimmer's Hand in a Swimming Competition. J Sports Sci Med. 12: 679-689.

Schleihauf R. 1979. A hydrodynamic analysis of swimming propulsion. Swimming III. University Park Press, Baltimore, 70–109.

Takagi H, Sanders R. 2002. Measurement of propulsion by the hand during competitive swimming. In The Engineering of Sport 4 (Eds. Ujihashi, S and Haake, SJ), 631-637, Blackwell Publishing.

Takagi H, Nakashima M, Ozaki T, Matsuuchi K. 2014. Unsteady hydrodynamic forces acting on a robotic arm and its flow field: Application to the crawl stroke. J Biomech. 47: 1401-1408.

Takagi H, Nakashima M, Sato Y, Matsuuchi K, Sanders RH. 2016. Numerical and experimental investigations of human swimming motions. J Sports Sci. 34(16): 1564-1580.

Toussaint HM, Berg CVD, Beek WJ. 2002. "Pumped-up propulsion" during front crawl swimming. Med Sci Sports Exerc. 34(2): 314–319.

Wilcox DC. 1988. Reassessment of the scale-determining equation for advanced turbulence models. AIAA J. 26(11):1299–1310.

Zaïdi H, Taïar R, Fohanno S, Polidori G. 2008. Analysis of the effect of swimmer's head position on swimming performance using computational fluid dynamics. J Biomech. 41: 1350–1358.